Journal of Photochemistry and Photobiology A: Chemistry 221 (2011) 214–219

Contents lists available at ScienceDirect

Journal of Photochemistry and Photobiology A: Chemistry

journal homepage: www.elsevier.com/locate/jphotochem

Electron transfer between methyl viologen radicals and graphene oxide: Reduction, electron storage and discharge

Sachidananda Krishnamurthy, Ian V. Lightcap, Prashant V. Kamat*

Radiation Laboratory and Departments of Chemistry and Biochemistry and Chemical & Biomolecular Engineering, University of Notre Dame, Notre Dame, IN 46556, United States

ARTICLE INFO

Article history:
Available online 26 February 2011

Keywords:
Graphene oxide
Methyl viologen
Electron transfer
Silver nanoparticles
Graphene–metal
Nanocomposites

ABSTRACT

Photochemically generated methyl viologen radicals undergo electron transfer with graphene oxide (GO) in ethanol suspensions. This charge transfer interaction results in the reduction of GO as well as storage of electrons. The stored electrons can be utilized to reduce Ag^+ ions and thus anchor silver nanoparticles on reduced graphene oxide (RGO). The spectroscopic experiments that elucidate the quantitative electron transfer and transmission electron microscopy that highlights the potential of designing metal–RGO assemblies are discussed.

1. Introduction

Graphene based assemblies are gaining attention because of their potential in designing electronic, sensing, and energy conversion devices [1–5]. The graphene oxide (GO) synthesized from chemical oxidation of graphite provides a simple and convenient method to obtain exfoliated, two-dimensional carbon sheets [6]. Oxidation diminishes graphene's excellent conducting properties, so reduction of GO is desirable in order to partially restore its sp^2 network [7]. Reduced graphene oxide (RGO) can be produced through chemical [7–9], sonolytic [10], microwave [11,12], photothermal [13,14], photocatalytic [15–18], and electrochemical methods [19,20].

Carbon nanostructures serve as excellent supports to anchor catalyst particles [5]. For example, electrocatalyst nanoparticles anchored on carbon nanotubes [21] and graphene [9] have been found to be useful in improving the performance of fuel cells. One interesting application of RGO is in the development of conducting scaffold for anchoring metal and semiconductor nanoparticles. Utilization of GO to store and shuttle electrons has been reported recently [22].

The functional groups of GO provide a convenient way to modify chemical properties of graphene-based systems. In particular, one can introduce semiconducting property by reacting with radicals [23,24]. In addition, GO also interacts noncovalently with planar organic molecules via electrostatic, π–π, or van der Waals interactions [25]. Interaction of RGO with pyrenebutyrate, rhodamine 6G, porphyrin and thiophene derivatives are often marked by fluorescence quenching of the organic molecule [26–30]. Charge transfer interaction between reduced graphene oxide and porphyrin derivative has been reported recently [31]. We report here the interaction between photochemically generated methyl viologen radicals ($MV^{\bullet}$) and GO and quantification of the electron transfer processes mediated by GO (Fig. 1).

2. Experimental

2.1. Materials

All chemicals (reagent grade) were purchased from Aldrich and used as supplied. Graphite powder, synthetic, conducting grade, 325 mesh, 99.9995% (metals basis) was obtained from Alfa Aesar. Graphene oxide was prepared by modified Hummers method [6]. Two grams of commercially available graphite powder, 1 g sodium nitrate ($NaNO_3$) and 46 mL sulphuric acid (H_2SO_4) were added while stirring to a 250 mL flask kept in an ice bath. Slowly, 6 g of potassium permanganate ($KMnO_4$) was added, taking care that the temperature of the solution did not rise above ~20 °C. The flask was removed from the ice bath and the temperature was increased to ~35 °C. The reaction vessel was maintained at this temperature for ~45 min during which time the solution became thicker and brownish-gray in color. 100 mL of water was then added in small increments. Care was taken to maintain the temperature of the solution below 100 °C. This elevated temperature was maintained for 15 min as the solution turned brown in color. 100 mL of 3% hydrogen peroxide was then added to the reaction vessel and the

* Corresponding author. Tel.: +1 574 631 5411.
E-mail addresses: kamat.1@nd.edu, PKAMAT@ND.edu (P.V. Kamat).

1010-6030/$ – see front matter © 2011 Elsevier B.V. All rights reserved.
doi:10.1016/j.jphotochem.2011.02.024

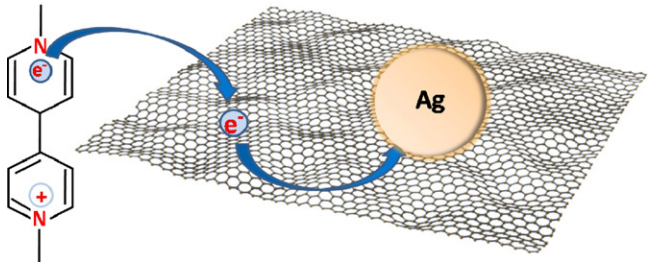

Fig. 1. Illustration depicting electron transfer from methyl viologen radical to graphene oxide and shuttling electrons through the carbon network to reduce Ag^+ ions to grow Ag nanoparticles.

reaction mixture was stirred for about 30 min at 80 °C. The reaction mixture was filtered to separate the brown colored graphene oxide solid. Graphene oxide was washed three times with both 1 M HCl and with DI water. The solid was transferred into an evaporating dish and dried at 60 °C and stored.

2.2. Preparing GO and RGO dispersions

Known amount of graphene oxide was dispersed in ethanol to obtain desired concentration. Reduced graphene oxide was obtained by dispersing 2 mg GO in 4 mL ethanol (or 0.5 mg GO/mL) and exposing the solution to unfiltered UV light (150 W Xenon lamp,) for 2 h with continuous stirring. The color of the dispersion turned from brown to black as the irradiation continued, indicating the reduction of GO to RGO.

2.3. Generating $MV^{+\bullet}$ radical and sequential transfer of electrons to GO and Ag^+

4 mL of 100 μM $MV^{2+}$was placed in a quartz cuvette and capped with a septum. The solution was deaerated for 40 min by N_2 purging and then irradiated with UV light for 15 s at which point the solution turned blue. The concentration of $MV^{+\bullet}$ was determined (usually ~40 μM) from the absorbance at 605 nm GO dispersion in ethanol was separately degassed for 40 min. Deaerated GO suspension (0.5 mg/mL) was added in increments of 10 μL to $MV^{+\bullet}$ solution to record the spectral changes. Addition of GO to $MV^{+\bullet}$ solution continued until the absorbance peak at 605 nm was eliminated. Titration of electrons stored in GO was estimated using Ag^+ titration as established previously [22]. 1 mM Ag^+ in ethanol was deaerated by purging with N_2 for 40 min. Deaerated Ag^+ solution (1 mM) was added in increments of 25 μL to the MV^{2+} – RGO(e) suspension and spectra were recorded. The growth of the plasmon absorption at 420 nm represents formation of Ag nanoparticles. The end point of electron titration corresponds to the breakpoint at which no additional increase (or saturation in the absorbance) in the 420 nm peak can be seen.

2.4. Methods

All solutions and dispersions were prepared using 200 proof ethanol. All experiments were carried out at room temperature (298 K) and in nitrogen atmosphere. Absorption spectra were measured with Varian Cary 50-Bio UV–Vis spectrophotometer or double beam Shimadzu UV-3101PC spectrophotometer. TEM micrographs were taken using FEI Titan 300 kV field emission TEM with Gatan Image Filter.

3. Results and discussion

3.1. Photochemical production of $MV^{+\bullet}$ and transfer of electrons to GO

Methyl viologen dissolved in deaerated ethanol was reduced under UV irradiation. The excited methyl viologen is reduced by ethanol and the formation of reduced product can be visualized from the blue coloration of the solution (reaction (1)). The reduction product accumulates in solution as we continue the UV-irradiation. The desired concentration of $MV^{+\bullet}$ was attained by controlling the duration of illumination. The details of the reduction of MV^{2+} in ethanol can be found elsewhere [32].

$$MV^{2+} + C_2H_5OH + h\nu \rightarrow MV^{+\bullet} + C_2H_5O^{\bullet} \quad (1)$$

Since $C_2H_5O^{\bullet}$ also serves as a reducing agent, we continue to accumulate $MV^{+\bullet}$ during the UV-irradiation. The $MV^{+\bullet}$ generated by photochemical reduction method remains stable in deaerated solutions and thus provides a convenient method to study the electron transfer processes in the absence of irradiation. The absorption spectrum *a* in Fig. 2A shows the spectral characteristics of $MV^{+\bullet}$ formed upon UV irradiation of 100 μM MV^{2+} in deaerated ethanol solution. $MV^{+\bullet}$ exhibits characteristics absorption 398 nm ($\varepsilon = 41{,}100\ M^{-1}\ cm^{-1}$) and 605 nm ($\varepsilon = 13{,}800\ M^{-1}\ cm^{-1}$) [32]. By controlling the time of irradiation we can control the amount of $MV^{+\bullet}$ formed in the solution. The absorbance of 0.55 at 605 nm which corresponds to 40 μM of $MV^{+\bullet}$ can be attained by irradiating deaerated solution of 100 μM MV^{2+} for 15 s.

Upon incremental addition of deaerated GO suspension to $MV^{+\bullet}$ solution we see a decrease in the absorbance of bands corresponding to $MV^{+\bullet}$. The spectra *b–h* show disappearance of $MV^{+\bullet}$ absorption band with continued addition of GO solution. Upon addition of 35 μg of GO we see complete disappearance of $MV^{+\bullet}$. Since the absorption change represents the disappearance of $MV^{+\bullet}$ and corresponding electron transfer process (reaction (2)), we can estimate the number of electrons transferred to GO. The inset in Fig. 2A shows the number of moles of electrons transferred versus concentration (in μg) of GO added. Based on the slope of the linear region of this plot we estimate transfer of 0.0047 μmol of electrons per μg of GO.

The results in Fig. 2A establish the quantitative transfer of electrons to GO. Whereas a fraction of these electrons are utilized in the reduction of GO to RGO, the rest of the transferred electrons are stored within RGO (reaction (2)),

$$nMV^{+\bullet} + mGO \rightarrow nMV^{2+} + mRGO[(n-m)e] \quad (2)$$

where *n* is the total electrons available for transfer and *m* is the number of reducible sites on GO. The excess electrons $(n-m)$ thus remain as stored on RGO and can be extracted with another electron acceptor.

To further verify the electron transfer from $MV^{+\bullet}$ to GO, we performed *in situ* reduction of GO in a suspension containing MV^{2+} under UV irradiation. As per reaction (1) UV illumination results in the formation of $MV^{+\bullet}$, part of which participates in the electron transfer with GO. Fig. 2(B) shows changes in the absorbance of GO before and after the electron transfer from $MV^{+\bullet}$. The increase in the absorbance is attributed to the partial restoration of the sp^2 network and thus confirms the reduction of GO [33].

We also performed the steady state UV-irradiation experiment to monitor the formation of $MV^{+\bullet}$ radical in ethanol solution in the presence and absence of GO and RGO. The absorbance at 605 nm, which is proportional to the concentration of $MV^{+\bullet}$, attains saturation as the system reaches steady state. It is interesting to note that the rate of growth as well as the steady state concentration is affected by the presence of GO (and RGO). The initial step involves reduction of GO while in the later stages it results in storage of elec-

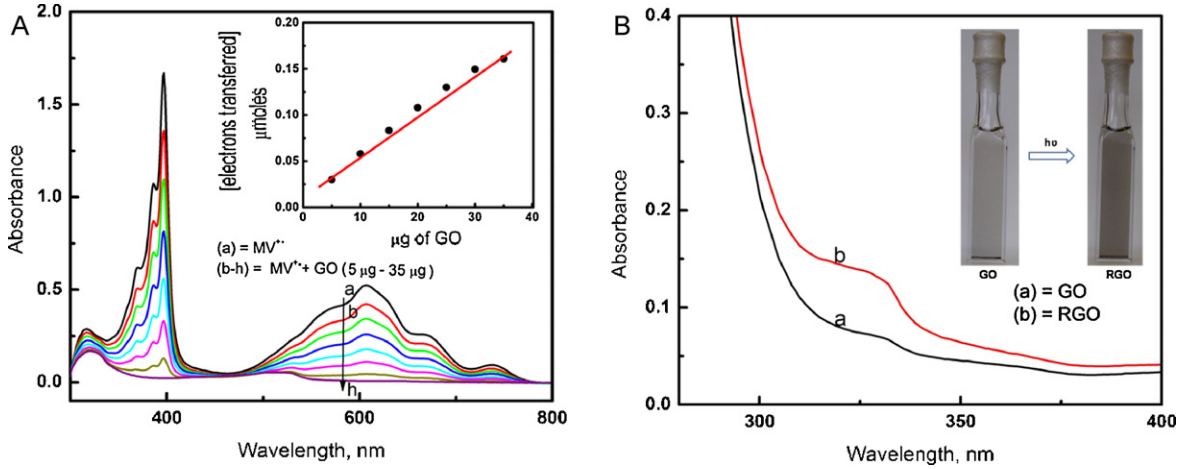

Fig. 2. (A) (a) Absorption spectrum of $MV^{+\bullet}$ formed following the UV irradiation of 100 μM MV^{2+} in deaerated ethanol (vol. 4 mL). Spectra *b*–*h* were recorded with increasing GO concentrations (increments of 10 μL of 0.5 mg/mL GO in ethanol was added to 4 mL $MV^{+\bullet}$ solution, viz., sample 'a'). Corresponding GO suspension in ethanol was used as a reference. Inset shows the number of electrons transferred versus μg of GO added. (B) Absorbance spectra of 50 μg GO in 4 mL MV^{2+} (a) before irradiation and (b) after irradiation and reduction with $MV^{+\bullet}$ in deaerated solution and then exposing to air. Inset shows the photographs showing the color change of 50 μg GO in 4 mL MV^{2+} before and after reduction.

trons. The charges between $MV^{+\bullet}$ and RGO are distributed under steady state irradiation as the two systems attain Fermi level equilibration. Such a charge equilibration phenomenon is similar to the one observed between $MV^{+\bullet}$ radical and carbon nanotubes [34]. The difference in absorbance (i.e., in the absence and presence of GO) corresponds to net loss of electrons from $MV^{+\bullet}$ and its accumulation in RGO under steady state irradiation condition. In the present experiment we estimate 0.044 μmol of electrons in 50 μg GO to be in equilibrium with 0.44 μM of $MV^{+\bullet}$ and 56 μM of MV^{2+}. Based on these equilibrated concentration of $MV^{+\bullet}$ and MV^{2+}, and using Nernst equation, we estimate the apparent Fermi level of RGO to be −0.44 V vs. NHE (Fig. 3).

3.2. Titration of stored electrons

In our earlier study, we have shown that RGO is capable of storing electrons that were transferred from excited TiO_2 particles [17,35]. The electron storage is facilitated by the double layer charging effects. Similar charging effects have been seen for CNT and Au nanoparticles [36,37]. One convenient way to probe these stored electrons is to utilize them for the reduction of silver ions [22].

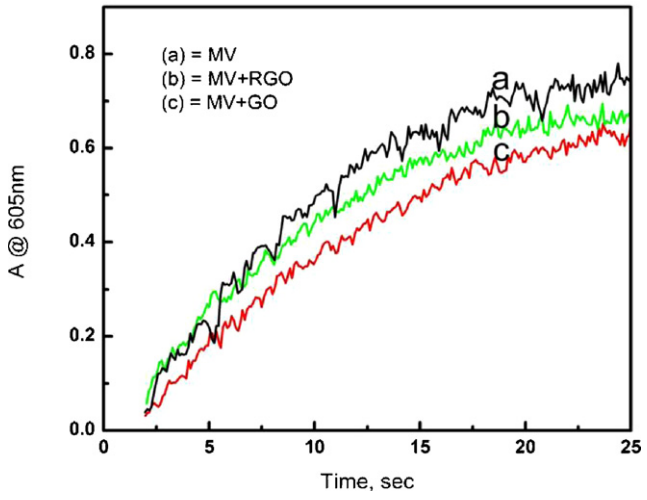

Fig. 3. Growth of absorbance at 605 nm following the UV irradiation of 100 μM MV^{2+} in ethanol (a) in the absence of GO or RGO (b) in the presence of 50 μg RGO in 4 mL MV^{2+} and (c) in the presence of 50 μg GO in 4 mL MV^{2+}.

The formation of silver nanocrystallites was monitored from the appearance of an absorption band at 420 nm. In order to estimate the stored electrons in the present experiments, we added known amounts of Ag^+ ions as electron scavengers (reaction (3)).

$$(n-m)\text{RGO} + Ag^+ \rightarrow \text{RGO} + Ag_{(n-m)} \quad (3)$$

Fig. 4A shows the absorption spectra recorded following the incremental addition of known amounts of Ag^+ to a solution of previously irradiated MV^{2+} along with subsequent GO addition (sample corresponding to *h* in Fig. 2A). With increasing addition of Ag^+ we see an increase in the absorption in the 400–420 nm region. This increase in the absorption represents formation of Ag nanoparticles. Once all electrons stored in GO are consumed, further addition of Ag^+ does not lead to growth in 420 nm absorption. The peak at 520 nm appears to arise from $MV^{+\bullet}$ radicals undergoing dimerization or related photoproduct formation [38].

Fig. 4B shows the increase in 420 nm absorption recorded with increasing Ag^+ concentration under three different experimental conditions. In the presence of GO and RGO we see a saturation in the 420 nm absorption band upon addition of 0.025 μmol of Ag^+. Further addition of Ag^+ results in little or no increase in absorption. The lower saturation value of absorbance observed in the case of GO is reflects lower electron storage capacity and/or utilization of electrons in the partial reduction of GO. As shown earlier [22], few Ag nanoparticle seeds are formed initially on the GO (or RGO) surface. Further addition of Ag^+ results in the growth of these seeds, and crystallite diameters as large as 200 nm have been observed. The sequential reduction of GO to RGO and electron transfer from RGO to Ag^+ is shown in Fig. 5. The visible changes in color of the suspension support the sequential electron transfer discussed in Figs. 2 and 4.

In the absence of GO or RGO, we observe a threshold for direct Ag^+ reduction by $MV^{+\bullet}$. Until 0.035 μmol of Ag^+ is added we see little change in 420 nm absorption. We see a quick rise in 420 nm absorption upon further addition of Ag^+. The lack of heterogeneous surface makes the initial seeding of Ag nanoparticles difficult. However, once a few seeds are formed they quickly catalyze the reduction of excess Ag^+ ions present in solution. The sharp increase in the absorption seen at 0.035 μmol of Ag^+ indicates that all available electrons are utilized instantly in the reduction process. In contrast, the reduction of Ag^+ on GO–RGO surface is slow and continuous. The results presented in Fig. 4B highlight the role of GO/RGO as a catalytic surface to promote the reduction of Ag^+ and

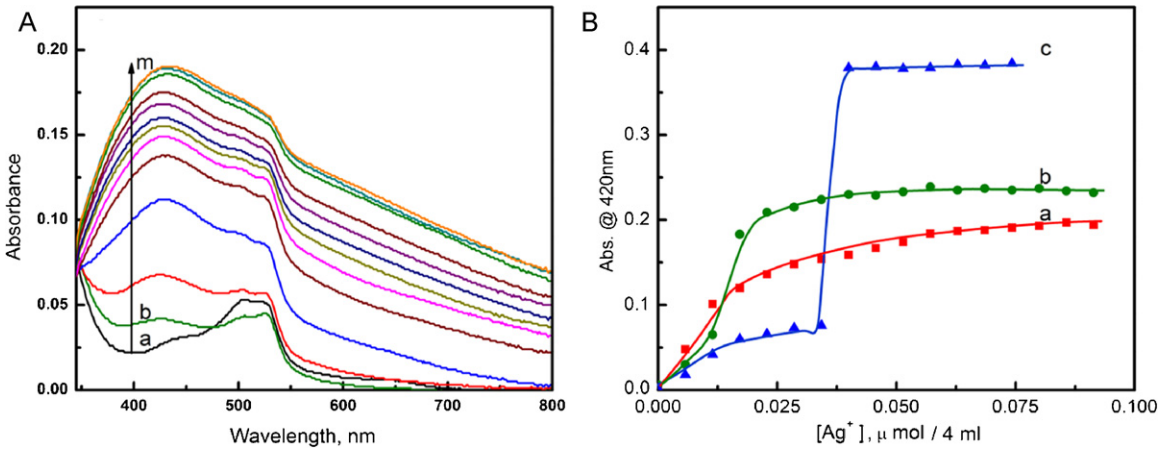

Fig. 4. (A) Absorption spectra recorded following the incremental addition of Ag^+ solution to [MV^{2+} + RGO(e)] in ethanol. Spectrum *a* corresponds to spectrum *h* in Fig. 2A. Spectra *b*–*m* were recorded with addition of Ag^+ (increments of 25 μL of 1 mM Ag^+ to 4 mL ethanol solution of MV^{2+} + RGO(e)). (B) The increase in absorbance at ~420 nm versus μmol of added Ag^+ (a) in the presence of GO and (b) in the presence of RGO. (c) Blank experiment carried out in the absence of GO or RGO.

growth of Ag nanoparticles. As shown earlier, the epoxide sites usually provide anchoring centers for Ag^+ and promote their reduction by shuttling electrons to these sites [39,40]. GO/RGO enabled growth of Ag nanoparticles further supports our earlier conclusion of electron transfer and storage at flat carbon surfaces.

3.3. TEM characterization

The results discussed in earlier sections show the spectroscopic fingerprint highlighting the reduction of GO by $MV^{+\bullet}$ followed by reduction of Ag^+. In order to further assess the morphology of RGO/Ag composites, we performed TEM measurements. Fig. 6A is a defocused bright field image showing a typical GO sheet on a holey carbon grid. Most sheets are single to few layers and have dimensions in micrometers. Even though oxidized, GO sheets retain sufficient periodicity in their conjugated network to display the characteristic diffraction pattern of pristine graphene, as seen in the inset. Since electrons are being stored on RGO sheets, this sp^2 network should allow for delocalized storage of charge. This effect is confirmed in TEM image Fig. 6B, which shows good dispersion of Ag nanoparticles on the graphene sheet with average diameter of ~30 nm. Ag nanoparticles reduced by $MV^{+\bullet}$ alone show greater size dispersion, with diameters ranging from 5 to 100 nm, and tend to agglomerate (Fig. 6D).

The effect of GO reduction by $MV^{+\bullet}$ is evident when comparing Fig. 6B and C. In Fig. 6C, pre-reduced RGO was used in the stepwise electron transfer. Electrons transferred from $MV^{+\bullet}$ therefore were all able to be stored, whereas in Fig. 6B, many of the elec-

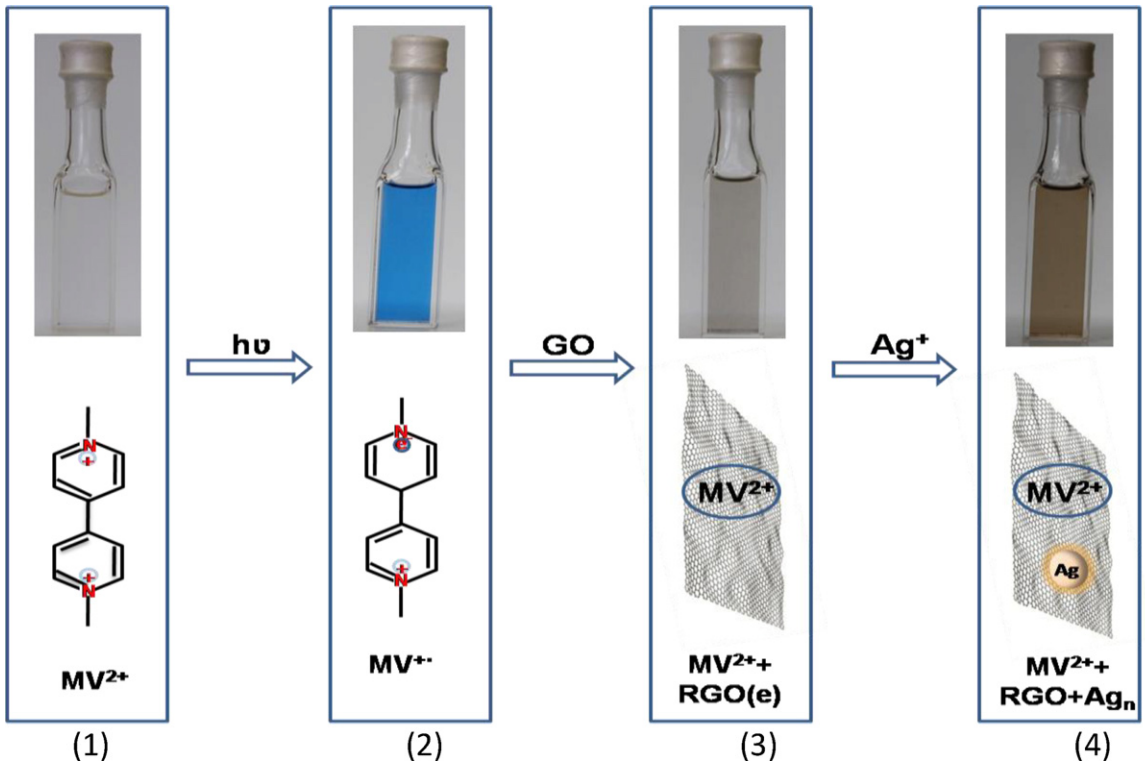

Fig. 5. Photographs showing the color changes observed after stepwise electron transfer along with the corresponding structures. (1) MV^{2+} in deaerated ethanol. (2) $MV^{+\bullet}$ in deaerated ethanol (upon irradiation of MV^{2+} with UV light for 15 s). (3) Electrons transferred to GO from $MV^{+\bullet}$ (upon addition of deaerated GO dispersion in ethanol). (4) Ag nanoparticles on RGO (upon addition of deaerated $AgNO_3$ solution in ethanol).

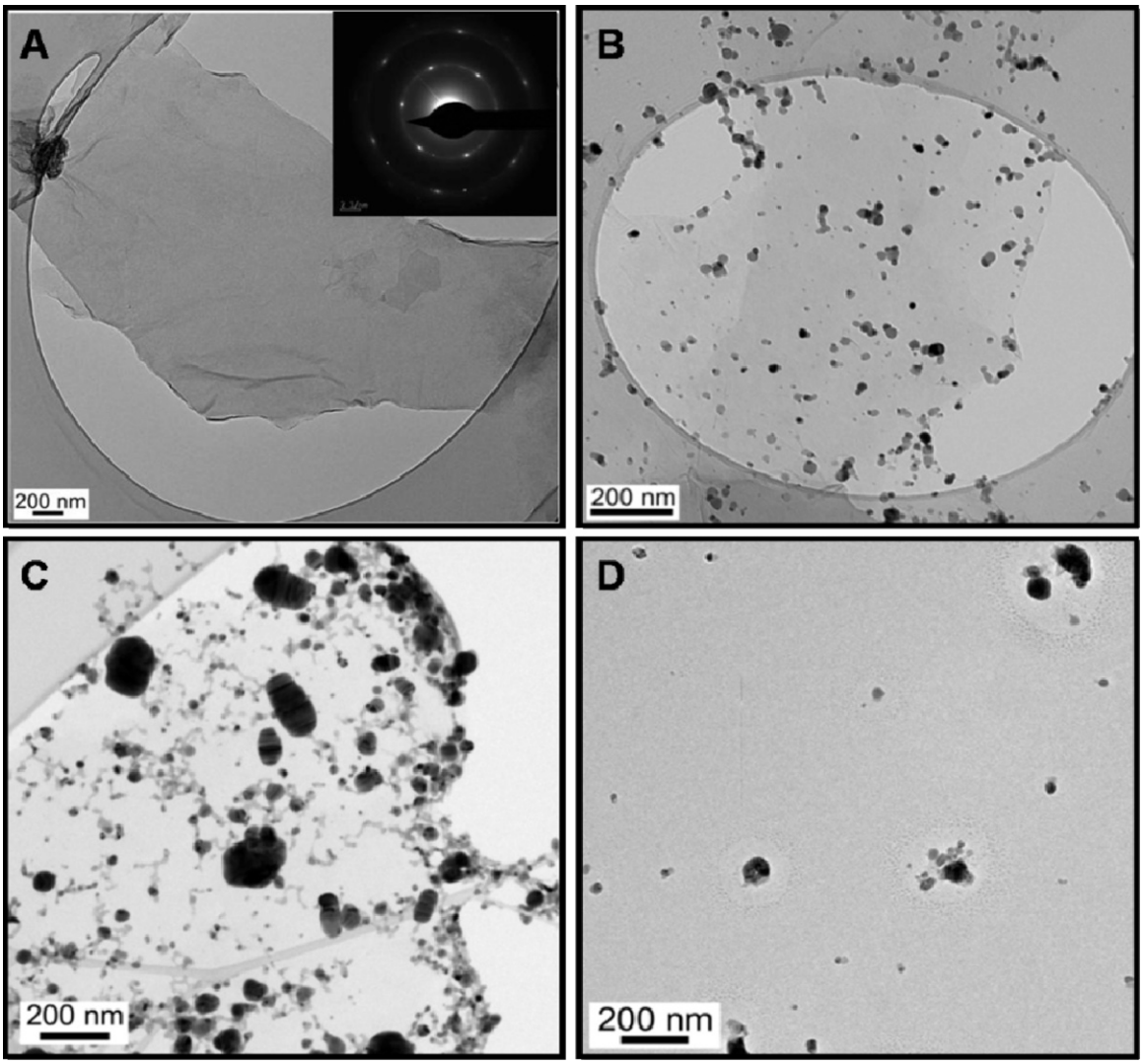

Fig. 6. (A) TEM image of GO sheet over holey carbon grid. Inset is the characteristic diffraction pattern of graphene, with reciprocal lattice spacings of 1.23 Å and 2.13 Å. (B) Ag nanoparticles dispersed on GO sheet. GO sheet reduced through e^- transfer from $MV^{+\bullet}$. Additional electrons transferred from $MV^{+\bullet}$ are stored in graphene sheet and are used for Ag^+ reduction and concurrent nanoparticle deposition. Average Ag nanoparticle diameter is ~30 nm. (C) RGO sheet with Ag nanoparticles up to 200 nm in diameter. Larger nanoparticle size is observed as all e^- transferred from $MV^{+\bullet}$ to RGO sheet are stored, then used to reduce Ag^+ ions. (D) Ag nanoparticles reduced directly by $MV^{+\bullet}$. (The experimental conditions were similar to Fig. 4B at the highest concentration level of Ag^+.)

trons are used in the reduction of GO. Using pre-reduced GO should thus result in a larger number of electrons stored and subsequently, larger Ag nanoparticle deposition upon reduction of Ag^+. This effect can be clearly seen as Ag nanoparticles on the pre-reduced RGO are larger, with several particles up to 200 nm in diameter per sheet (Fig. 6C).

4. Conclusions

Methyl viologen radicals are capable of transferring electrons to graphene oxide and partially restore the sp^2 network. The reduced graphene oxide serves as a scaffold to anchor Ag nanoparticles. The growth of these silver nanoparticles is dictated by the ability of RGO to store and shuttle electrons. The RGO/Ag nanocomposites discussed in the present work offer new opportunities to design next generation photocatalysts.

Acknowledgments

The financial support of the Department of Energy, Office of Basic Energy Sciences is gratefully acknowledged. This is contribution number NDRL-4874 from the Notre Dame Radiation Laboratory.

References

[1] A.K. Geim, Graphene: status and prospects, Science 324 (2009) 1530–1534.
[2] P.V. Kamat, Graphene-based nanoassemblies for energy conversion, J. Phys. Chem. Lett. 2 (2011) 242–251.
[3] C.N.R. Rao, A.K. Sood, R. Voggu, K.S. Subrahmanyam, Some novel attributes of graphene, J. Phys. Chem. Lett. 1 (2010) 572–580.
[4] M.H. Liang, B. Luo, L.J. Zhi, Application of graphene and graphene-based materials in clean energy-related devices, Int. J. Energy Res. 33 (2009) 1161–1170.
[5] P.V. Kamat, Graphene based nanoarchitectures anchoring semiconductor and metal nanoparticles on a 2-dimensional carbon support, J. Phys. Chem. Lett. 1 (2010) 520–527.
[6] W.S. Hummers, R.E. Offeman, Preparation of graphitic oxide, J. Am. Chem. Soc. 80 (1958) 1339–1439.
[7] S. Park, R.S. Ruoff, Chemical methods for the production of graphenes, Nat. Nanotechnol. 4 (2009) 217–224.
[8] R. Muszynski, B. Seger, P. Kamat, Decorating graphene sheets with gold nanoparticles, J. Phys. Chem. C 112 (2008) 5263–5266.
[9] B. Seger, P.V. Kamat, Electrocatalytically active graphene–platinum nanocomposites role of 2-D carbon support in PEM fuel cells, J. Phys. Chem. C 113 (2009) 7990–7995.
[10] K. Vinodgopal, B. Neppolian, I.V. Lightcap, F. Grieser, M. Ashokkumar, P.V. Kamat, Sonolytic design of graphene Au nanocomposites simultaneous and

sequential reduction of graphene oxide and Au(III), J. Phys. Chem. Lett. 1 (2010) 1987–1993.
[11] H.M.A. Hassan, V. Abdelsayed, A.E.R.S. Khder, K.M. AbouZeid, J. Terner, M.S. El-Shall, S.I. Al-Resayes, A.A. El-Azhary, Microwave synthesis of graphene sheets supporting metal nanocrystals in aqueous and organic media, J. Mater. Chem. 19 (2009) 3832–3837.
[12] A.F. Zedan, S. Sappal, S. Moussa, M.S. El-Shall, Ligand-controlled microwave synthesis of cubic and hexagonal CdSe nanocrystals supported on graphene photoluminescence quenching by graphene, J. Phys. Chem. C 114 (2010) 19920–19927.
[13] V. Abdelsayed, S. Moussa, H.M. Hassan, H.S. Aluri, M.M. Collinson, M.S. El-Shall, Photothermal deoxygenation of graphite oxide with laser excitation in solution and graphene-aided increase in water temperature, J. Phys. Chem. Lett. 1 (2010) 2804–2809.
[14] D.A. Sokolov, K.R. Shepperd, T.M. Orlando, Formation of graphene features from direct laser-induced reduction of graphite oxide, J. Phys. Chem. Lett. 1 (2010) 2633–2636.
[15] Y.H. Ng, I.V. Lightcap, K. Goodwin, M. Matsumura, P.V. Kamat, To what extent do graphene scaffolds improve the photovoltaic and photocatalytic response of TiO_2 nanostructured films? J. Phys. Chem. Lett. 1 (2010) 2222–2227.
[16] Y.H. Ng, A. Iwase, A. Kudo, R. Amal, Reducing graphene oxide on a visible-light $BiVO_4$ photocatalyst for an enhanced photoelectrochemical water splitting, J. Phys. Chem. Lett. 1 (2010) 2607–2612.
[17] G. Williams, B. Seger, P.V. Kamat, TiO_2–graphene nanocomposites UV-assisted photocatalytic reduction of graphene oxide, ACS Nano 2 (2008) 1487–1491.
[18] G. Williams, P.V. Kamat, Graphene-semiconductor nanocomposites excited state interactions between ZnO nanoparticles and graphene oxide, Langmuir 25 (2009) 13869–13873.
[19] G.K. Ramesha, S. Sampath, Electrochemical reduction of oriented graphene oxide films: an in situ Raman spectroelectrochemical study, J. Phys. Chem. C 113 (2009) 7985–7989.
[20] S.J. An, Y. Zhu, S.H. Lee, M.D. Stoller, T. Emilsson, S. Park, A. Velamakanni, J. An, R.S. Ruoff, Thin film fabrication and simultaneous anodic reduction of deposited graphene oxide platelets by electrophoretic deposition, J. Phys. Chem. Lett. 1 (2010) 1259–1263.
[21] A. Kongkanand, K. Vinodgopal, S. Kuwabata, P.V. Kamat, Highly-dispersed Pt catalysts on single-walled carbon nanotubes and their role in methanol oxidation, J. Phys. Chem. B 110 (2006) 16185–16192.
[22] I.V. Lightcap, T.H. Kosel, P.V. Kamat, Anchoring semiconductor and metal nanoparticles on a 2-dimensional catalyst mat storing and shuttling electrons with reduced graphene oxide, Nano Lett. 10 (2010) 577–583.
[23] E. Bekyarova, M.E. Itkis, P. Ramesh, R.C. Haddon, Chemical approach to the realization of electronic devices in epitaxial graphene, Phys. Stat. Solidi-Rapid Res. Lett. 3 (2009) 184–186.
[24] E. Bekyarova, M.E. Itkis, P. Ramesh, C. Berger, M. Sprinkle, W.A. de Heer, R.C. Haddon, Chemical modification of epitaxial graphene: spontaneous grafting of aryl groups, J. Am. Chem. Soc. 131 (2009) 1336–1337.
[25] A. Das, S. Pisana, B. Chakraborty, S. Piscanec, S.K. Saha, U.V. Waghmare, K.S. Novoselov, H.R. Krishnamurthy, A.K. Geim, A.C. Ferrari, A.K. Sood, Monitoring dopants by Raman scattering in an electrochemically top-gated graphene transistor, Nat. Nanotechnol. 3 (2008) 210–215.
[26] Y.X. Xu, H. Bai, G.W. Lu, C. Li, G.Q. Shi, Flexible graphene films via the filtration of water-soluble noncovalent functionalized graphene sheets, J. Am. Chem. Soc. 130 (2008) 5856–5857.
[27] J. Geng, H.-T. Jung, Porphyrin functionalized graphene sheets in aqueous suspensions: from the preparation of graphene sheets to highly conductive graphene films, J. Phys. Chem. C 114 (2010) 8227–8234.
[28] L. Xie, X. Ling, Y. Fang, J. Zhang, Z. Liu, Graphene as a substrate to suppress fluorescence in resonance Raman spectroscopy, J. Am. Chem. Soc. 131 (2009) 9890–9891.
[29] X. Ling, L. Xie, Y. Fang, H. Xu, H. Zhang, J. Kong, M.S. Dresselhaus, J. Zhang, Z. Liu, Can graphene be used as a substrate for Raman enhancement? Nano Lett. 10 (2009) 553–561.
[30] E. Treossi, M. Melucci, A. Liscio, M. Gazzano, P. Samori, V. Palermo, High-contrast visualization of graphene oxide on dye-sensitized glass, quartz, and silicon by fluorescence quenching, J. Am. Chem. Soc. 131 (2009) 15576–15577.
[31] A Wojcik, P.V. Kamat, Reduced graphene oxide and porphyrin. An interactive affair in 2-D, ACS Nano 4 (2010) 6697–6706.
[32] T.W. Ebbesen, G. Ferraudi, Photochemistry of methyl viologen in aqueous and methanolic solutions, J. Phys. Chem. 87 (1983) 3717–3721.
[33] N.A. Kotov, I. Dekany, J.H. Fendler, Ultrathin graphite oxide–polyelectrolyte composites prepared by self-assembly: transition between conductive and non-conductive states, Adv. Mater. 8 (1996) 637–641.
[34] A. Kongkanand, P.V. Kamat, Interactions of single wall carbon nanotubes with methyl viologen radicals quantitative estimation of stored electrons, J. Phys. Chem. C 111 (2007) 9012–9015.
[35] P.V. Kamat, What makes semiconductor colloids unique as photocatalysts, Spectrum 6 (1993) 14–20.
[36] S. Chen, R.W. Murray, Electrochemical quantized capacitance charging of surface ensembles of gold nanoparticles, J. Phys. Chem. B 103 (1999) 9996–10000.
[37] M. Jakob, H. Levanon, P.V. Kamat, Charge distribution between UV-irradiated TiO_2 and gold nanoparticles. Determination of shift in Fermi level, Nano Lett. 3 (2003) 353–358.
[38] M. Wolszczak, C. Stradowski, Methyl viologen cation radical its dimer and complex in various media, Rad. Phys. Chem. 33 (1989) 355–359.
[39] K. Jasuja, V. Berry, Implantation growth of dendritic gold nanostructures on graphene derivatives: electrical property tailoring and Raman enhancement, Acs Nano 3 (2009) 2358–2366.
[40] K. Jasuja, J. Linn, S. Melton, V. Berry, Uncapped catalytically-enhanced solution-dispersed graphene supported metal nanoparticles grown via microwave reduction: tuning catalytic, electrical and Raman properties, J. Phys. Chem. Lett. 1 (2010) 1853–1860.